EUROPEAN ORGANIZATION FOR NUCLEAR RESEARCH (CERN)

CERN-EP-2021-182
LHCb-PAPER-2021-026
15 September 2021

Measurement of $\chi_{c1}(3872)$ production in proton-proton collisions at $\sqrt{s} = 8$ and 13 TeV

LHCb collaboration[†]

Abstract

The production cross-section of the $\chi_{c1}(3872)$ state relative to the $\psi(2S)$ meson is measured using proton-proton collision data collected with the LHCb experiment at centre-of-mass energies of $\sqrt{s} = 8$ and 13 TeV, corresponding to integrated luminosities of 2.0 and 5.4 fb^{-1}, respectively. The two mesons are reconstructed in the $J/\psi\pi^+\pi^-$ final state. The ratios of the prompt and nonprompt $\chi_{c1}(3872)$ to $\psi(2S)$ production cross-sections are measured as a function of transverse momentum, $p_{\rm T}$, and rapidity, y, in the kinematic range $4 < p_{\rm T} < 20$ GeV/c and $2.0 < y < 4.5$. The prompt ratio is found to increase with $p_{\rm T}$ independently of y. The double-differential cross-section ratio of $\chi_{c1}(3872)$ relative to $\psi(2S)$ mesons between 13 and 8 TeV is also measured for the prompt component and observed to be consistent with unity, independent of $p_{\rm T}$ and centre-of-mass energy.

Submitted to JHEP

[†]Authors are listed at the end of this paper.

1 Introduction

The $\chi_{c1}(3872)$ state was observed in the $J/\psi\pi^+\pi^-$ invariant-mass spectrum by the Belle collaboration in 2003 [1], and was subsequently confirmed by the BaBar, CDF and D0 collaborations [2–4]. Its quantum numbers have been determined to be $J^{PC} = 1^{++}$ by the LHCb collaboration [5]. Nevertheless, despite intense experimental and theoretical studies, the nature of the state is still unclear. The mass is close to the $D^0\overline{D}^{*0}$ threshold, which led to models where the $\chi_{c1}(3872)$ state is a $D^0\overline{D}^{*0}$ molecule with a very small binding energy [6, 7]. The LHCb collaboration indeed measured that the mass is slightly below that threshold [8, 9]. However, the differential production cross-section measured by the CMS collaboration [10] is lower than that predicted by non-relativistic QCD (NRQCD) [11] for the $D^0\overline{D}^{*0}$ molecule hypothesis. Alternatively, the $\chi_{c1}(3872)$ state can be interpreted as an admixture of $\chi_{c1}(2P)$ and $D^0\overline{D}^{*0}$ molecule states, produced through its $\chi_{c1}(2P)$ component. Under this hypothesis, a next-to-leading-order (NLO) NRQCD calculation [12] tuned to the results obtained by the CMS collaboration, agrees well with measurements performed by the ATLAS collaboration [13]. Recently, the ratio of prompt-production cross-sections between $\chi_{c1}(3872)$ and $\psi(2S)$ states produced directly from proton-proton (pp) collisions, as a function of multiplicity of the charged particles in event, has been measured by the LHCb collaboration using 8 TeV pp collision data [14]. This ratio is found to decrease with multiplicity. The interpretation of this observation is still unclear [15, 16].

In this paper, the double-differential production cross-section of the $\chi_{c1}(3872)$ state relative to that of the $\psi(2S)$ meson, where both decay to the $J/\psi\pi^+\pi^-$ final state, is measured using pp collision data collected by the LHCb detector at centre-of-mass energies of $\sqrt{s} = 8$ and 13 TeV. The cross-section is determined in intervals of the $J/\psi\pi^+\pi^-$ momentum transverse to the beam, $p_{\rm T}$, and rapidity, y, within the ranges $4 < p_{\rm T} < 20\,{\rm GeV}/c$ and $2.0 < y < 4.5$. The cross-section ratio $\sigma_{\chi_{c1}(3872)}/\sigma_{\psi(2S)}$ is measured separately for prompt and nonprompt production of the $\chi_{c1}(3872)$ and $\psi(2S)$ mesons, the latter occurring via b-hadron decays. In this ratio, the systematic uncertainties largely cancel. The production cross-section of the $\chi_{c1}(3872)$ state at a centre-of-mass energy of $\sqrt{s} = 7$ TeV has been previously measured [17]. Using the data recorded during the 2012 and 2016–2018 data-taking periods, corresponding to integrated luminosities of 2.0 and $5.4\,{\rm fb}^{-1}$, the signal yields increase by about a factor of 400, allowing a measurement of the double-differential cross-section to be performed for the first time.

2 Detector and simulation

The LHCb detector [18, 19] is a single-arm forward spectrometer covering the pseudorapidity range $2 < \eta < 5$, designed for the study of particles containing b or c quarks. The detector includes a high-precision tracking system consisting of a silicon-strip vertex detector surrounding the pp interaction region [20], a large-area silicon-strip detector located upstream of a dipole magnet with a bending power of about 4 Tm, and three stations of silicon-strip detectors and straw drift tubes [21, 22] placed downstream of the magnet. The tracking system provides a measurement of the momentum, p, of charged particles with a relative uncertainty that varies from 0.5% at low momentum to 1.0% at $200\,{\rm GeV}/c$. The minimum distance of a track to a primary pp-collision vertex (PV),

the impact parameter (IP), is measured with a resolution of $(15 + 29/p_{\rm T})\,\mu$m, with $p_{\rm T}$, in GeV/c. Different types of charged hadrons are distinguished using information from two ring-imaging Cherenkov (RICH) detectors [23]. The online event selection is performed by a trigger system [24], which consists of a hardware stage, based on information from the muon system, followed by a software stage, which is applied to apply a full event reconstruction. To reject high-multiplicity events with a large number of pp interactions, a set of global event requirements is applied on the hit multiplicities of subdetectors.

Simulated samples are used to develop the event selection and to estimate the detector acceptance and the efficiency of the imposed selection requirements. Simulated pp collisions are generated using Pythia [25] with a specific LHCb configuration [26]. Decays of unstable particles are described by EvtGen [27], in which final-state radiation is generated using Photos [28]. The interaction of the generated particles with the detector, and its response, are implemented using the Geant4 toolkit [29] as described in Ref. [30].

3 Event selection

The $\chi_{c1}(3872)$ and $\psi(2S)$ candidates are both reconstructed in the $J/\psi\pi^+\pi^-$ final state, with the J/ψ meson decaying into a pair of oppositely charged muons. At least one reconstructed primary vertex is required per event. Muon candidates are required to be well identified, and have $p_{\rm T} > 650\,{\rm MeV}/c$ and $p > 10\,{\rm GeV}/c$. Only reconstructed muon tracks of good quality are selected. The $\mu^+\mu^-$ pair is required to have a combined $p_{\rm T} > 3\,{\rm GeV}/c$ and an invariant mass in the range 3010–3170 MeV/c^2. The χ^2/ndf of the dimuon vertex fit is required to be less than 20, where ndf is the number of degrees of freedom.

Charged pion candidates are selected using particle identification (PID) information from the RICH detectors. The (transverse) momentum of the pions is required to be greater than (500) $3000\,{\rm MeV}/c$, while the pion track χ^2/ndf to be less than 4.

The $\chi_{c1}(3872)$ and $\psi(2S)$ candidates are reconstructed by combining each J/ψ candidate with a pair of oppositely charged pions. In order to improve the $J/\psi\pi^+\pi^-$ invariant-mass resolution, a vertex fit constraining the $\mu^+\mu^-$ invariant mass to the known J/ψ mass [31], $m_{J/\psi}$, is performed. The vertex fit χ^2/ndf is required to be less than 5. The decay energy release, $Q \equiv M_{J/\psi\pi^+\pi^-} - m_{J/\psi} - M_{\pi^+\pi^-}$, with $M_{J/\psi\pi^+\pi^-}$ and $M_{\pi^+\pi^-}$ being the invariant masses of, respectively, $J/\psi\pi^+\pi^-$ and $\pi^+\pi^-$ systems, is required to be less than $300\,{\rm MeV}/c^2$.

A pseudodecay-time of the $\chi_{c1}(3872)$ and $\psi(2S)$ candidates is constructed as

$$t_z = \frac{(z - z_{\rm PV}) \times m}{p_z}, \tag{1}$$

where z and $z_{\rm PV}$ are the candidate decay vertex and best-reconstructed PV positions along the beam (z) axis, p_z is the z component of the $\chi_{c1}(3872)$ or $\psi(2S)$ momenta, and m represents the known masses of these states [31]. Only candidates with $|t_z| < 10\,{\rm ps}$ are kept for further analysis. The pseudodecay-time of promptly produced $\chi_{c1}(3872)$ and $\psi(2S)$ mesons is zero, whereas that of mesons originating from b-hadron decays follows an exponential distribution. This variable is used to statistically discriminate between promptly and nonpromptly produced candidates.

4 Cross-section determination

The differential production cross-section of $\chi_{c1}(3872)$ relative to $\psi(2S)$ mesons times their ratio of branching ratios ($\mathcal{B}$) to the $J/\psi\pi^+\pi^-$ final state measured in $(p_{\rm T}, y)$ intervals is defined as

$$R \equiv \frac{\sigma_{\chi_{c1}(3872)}}{\sigma_{\psi(2S)}} \times \frac{\mathcal{B}(\chi_{c1}(3872) \to J/\psi\pi^+\pi^-)}{\mathcal{B}(\psi(2S) \to J/\psi\pi^+\pi^-)} = \frac{N_{\chi_{c1}(3872)}}{N_{\psi(2S)}} \times \frac{\epsilon_{\psi(2S)}}{\epsilon_{\chi_{c1}(3872)}}, \tag{2}$$

where $N_{\chi_{c1}(3872)}$ and $N_{\psi(2S)}$ are the observed signal yields of $\chi_{c1}(3872)$ and $\psi(2S)$ mesons, and $\epsilon_{\chi_{c1}(3872)}$ and $\epsilon_{\psi(2S)}$ are the total efficiencies, respectively. The yields of prompt $\chi_{c1}(3872)$ and $\psi(2S)$ mesons and those from b-hadron decays are determined in each $(p_{\rm T}, y)$ interval from a two-dimensional extended binned maximum-likelihood fit to the $J/\psi\pi^+\pi^-$ invariant-mass spectrum and the pseudodecay-time distribution.

For the invariant-mass model, the sum of two double-sided Crystal Ball (DSCB) functions [32] is used to describe the $\psi(2S)$ signal. The two DSCB functions share a common mean and have different width parameters. The relative fraction of the DSCB functions is determined from simulation. The radiative-tail parameters of the DSCB functions are parameterised as a function of the mass resolution, which is obtained using simulated samples. The combinatorial background in the $\psi(2S)$ signal window, defined by $M_{J/\psi\pi^+\pi^-}$ within the 3650–3720 MeV/c^2 interval, is described by an exponential function with the slope parameter freely varied. The fit function for the $\chi_{c1}(3872)$ signal is defined with a non-relativistic Breit–Wigner shape convolved with a invariant-mass resolution function, which has the same parameterisation as the $\psi(2S)$ signal. The worse signal-to-background ratio in the $\chi_{c1}(3872)$ mass region is mainly due to the fact that the production rate of $\chi_{c1}(3872)$ state is much smaller than that of the $\psi(2S)$ charmonium. The $\chi_{c1}(3872)$ mass is fixed to the known $m_{\psi(2S)}$ value [31] shifted by 185.49 MeV/c^2 [9], and its width is Gaussian constrained to 1.19 ± 0.19 MeV, which is the average value of two previous LHCb measurements [8, 9]. The ratios of the mass resolutions between the $\chi_{c1}(3872)$ and $\psi(2S)$ signals are determined from simulated samples. An exponential function is used to describe the combinatorial background in the $\chi_{c1}(3872)$ mass window, with $M_{J/\psi\pi^+\pi^-}$ between 3830 and 3910 MeV/c^2.

For the pseudodecay-time model, a delta function is used to describe the t_z distribution of the prompt $\chi_{c1}(3872)$ and $\psi(2S)$ signals, while an exponential function is used for that from b-hadron decays. Both are convolved with a resolution function chosen to be the sum of three Gaussian functions. The average peseudodecay-time of the nonprompt $\psi(2S)$ signal, referred to hereafter as pseudolifetime, is allowed to vary freely in the fit and found to be 1.5 ps with a mild dependence on the $\psi(2S)$ kinematics. Due to the high level of background in the $\chi_{c1}(3872)$ candidate sample, the pseudolifetime of nonprompt $\chi_{c1}(3872)$ candidates is fixed to 1.5 ps. It is possible that the reconstructed $\chi_{c1}(3872)$ or $\psi(2S)$ candidate is associated to a wrong PV, which would result in a long tail in the t_z distribution and would weakly contribute to the signal peak in the mass distribution. A nonparametric model is defined for this component by combining each signal candidate with the closest PV in a different event of the selected sample and taking the resulting t_z distribution as a template in the fit. The dominant background component is combinatorial, in which the J/ψ candidate is combined with a random pion pair uncorrelated with the signal candidate. The t_z distribution of the background in each $(p_{\rm T}, y)$ interval is obtained using the *sPlot* technique [33] with the mass as a

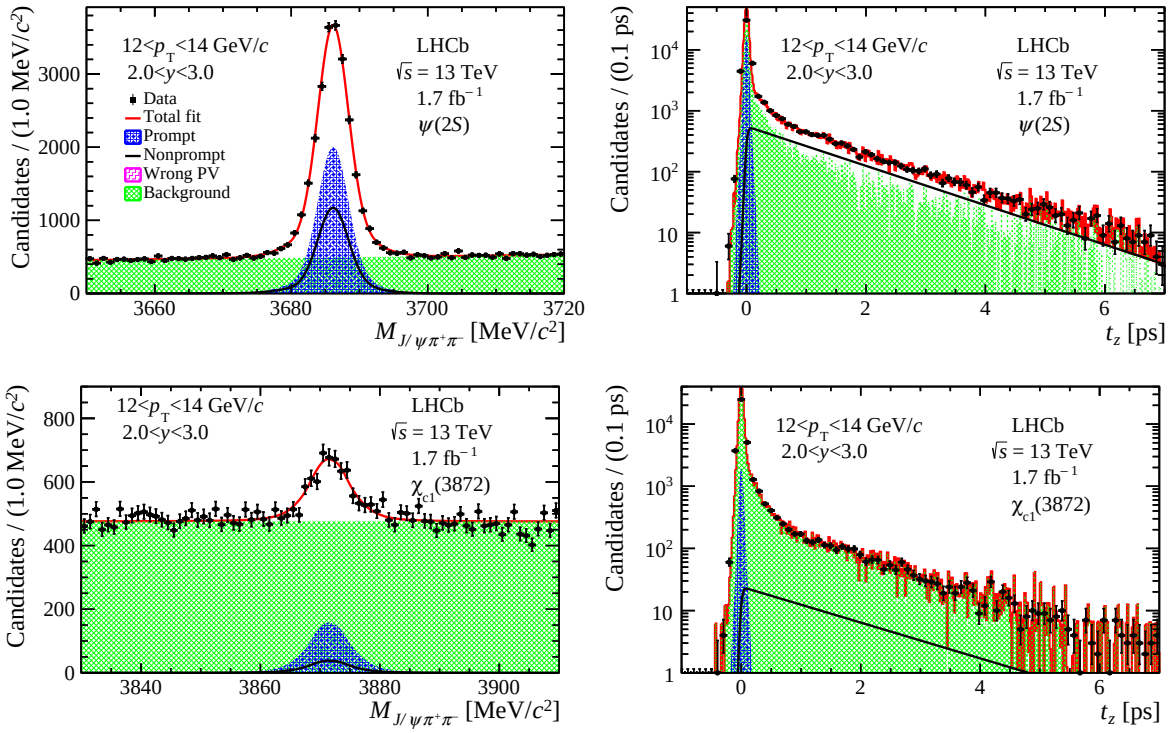

Figure 1: Distributions of (left) invariant mass and (right) pseudodecay-time for (top) $\psi(2S)$ and (bottom) $\chi_{c1}(3872)$ candidates in the kinematic interval $12 < p_{\rm T} < 14\,{\rm GeV}/c$ and $2.0 < y < 3.0$ for the 2016 data sample. Fit projections are overlaid. The solid red curve represents the total fit projection and the shaded green area corresponds to the background component. The prompt contribution of $\chi_{c1}(3872)$ and $\psi(2S)$ mesons is shown as the cross-hatched blue area, whereas the corresponding nonprompt component from b-hadron decays is illustrated as a solid black line. The wrong PV contribution is consistent with zero.

discriminating observable. The resulting model is fixed in the combined invariant mass and pseudodecay-time fit. The fit is performed separately for each data-taking year. As an example, Fig. 1 shows the $M_{J/\psi\pi^+\pi^-}$ and t_z distributions along with the fit projections for the 2016 data sample in the kinematic interval $12 < p_{\rm T} < 14\,{\rm GeV}/c$ and $2 < y < 3$.

The total efficiency in each kinematic interval is determined as the product of detector geometrical acceptance, particle reconstruction, event selection including trigger requirements, and particle identification efficiencies. The geometrical acceptance is calculated separately from $\chi_{c1}(3872)$ and $\psi(2S)$ simulated events. The track reconstruction and the particle-identification efficiencies are evaluated using simulated samples calibrated with data. The efficiencies for prompt and nonprompt $\chi_{c1}(3872)$ and $\psi(2S)$ signals are found to be slightly different, which is mainly caused by events containing b-hadron decays having larger occupancies and thus smaller tracking efficiencies. This effect does not affect the ratio of $\psi(2S)$ and $\chi_{c1}(3872)$ efficiencies, which is present in the cross-section ratio in Eq 2. The ratio of the total efficiencies of $\psi(2S)$ to $\chi_{c1}(3872)$ mesons is shown in Fig. 2 for the 2012 and 2016 data-taking periods, and the smaller efficiency at low $p_{\rm T}$ of the $\psi(2S)$ meson is due to its smaller mass.

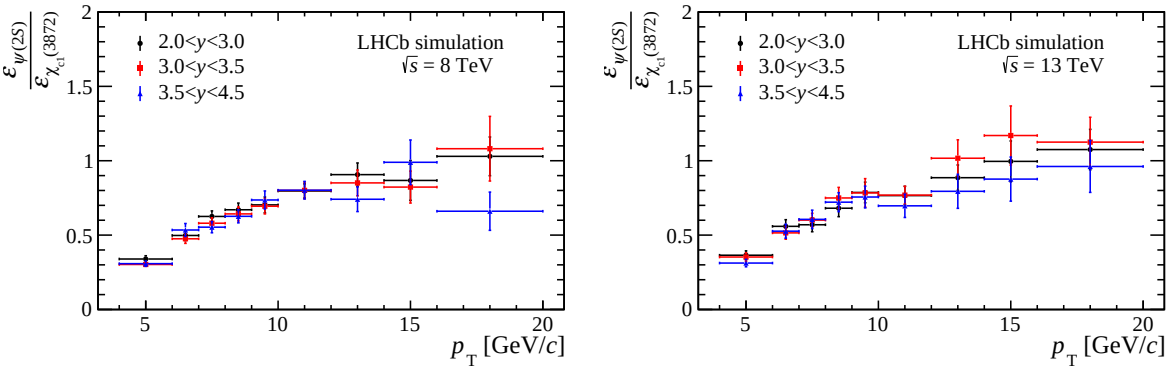

Figure 2: Efficiency ratio of $\psi(2S)$ to $\chi_{c1}(3872)$ mesons as a function of $p_{\rm T}$ in three rapidity intervals.

5 Systematic uncertainties

A variety of systematic uncertainty sources is studied and summarised in Table 1. The uncertainties arise from the $J/\psi\pi^+\pi^-$ invariant mass and pseudodecay-time fit models, and the computation of efficiencies. Some uncertainties depend on kinematics, with the largest values always appearing in the intervals with smaller sample sizes.

The signal lineshape chosen in the invariant-mass model can affect the measured signal yields. Such effects are evaluated using pseudoexperiments in which the signal description is taken from the simulated sample, and the background is generated with the shape and fraction determined from the fits to the data. The same fit model as used for the data is applied to these samples. The difference between the fitted value of the $N_{\chi_{c1}(3872)}/N_{\psi(2S)}$ ratio and the input value is taken as systematic uncertainty. In the default fit, the parameters of the fit model, such as the fraction of two DSCBs, the resolution ratios $\sigma_2^{\psi(2S)}/\sigma_1^{\psi(2S)}$ and $\sigma_i^{\chi_{c1}(3872)}/\sigma_i^{\psi(2S)}$ $(i=1,2)$ are determined from simulated samples and fixed in the fit to the data. Here, the $\sigma_2^{\psi(2S)}/\sigma_1^{\psi(2S)}$ represents the ratio of invariant-mass resolutions approximated as two Gaussian cores for the $\psi(2S)$ meson, and $\sigma_i^{\chi_{c1}(3872)}/\sigma_i^{\psi(2S)}$ $(i=1,2)$ is the ratio between the invariant-mass resolutions for the first or second Gaussian core of the $\psi(2S)$ and $\chi_{c1}(3872)$ mesons. These parameters are varied within their statistical uncertainties, and the average shift of the $N_{\chi_{c1}(3872)}/N_{\psi(2S)}$ ratio is assigned as uncertainty. The contributions to the systematic uncertainty due to the background mass shape are estimated by replacing the exponential function by a second-order polynomial function, and evaluating the difference of $N_{\chi_{c1}(3872)}/N_{\psi(2S)}$ between the alternative and the default fits.

There are several analysis choices that could affect the nonprompt fit fraction, F_b, and they are studied separately for each data-taking year. The first is the t_z resolution model. A sum of three Gaussian functions is used to describe the t_z resolution of the $\psi(2S)$ and $\chi_{c1}(3872)$ signal. As an alternative, a sum of two Gaussian functions is used, and the relative differences of the fitted F_b ratio for the $\chi_{c1}(3872)$ and $\psi(2S)$ signal, $F_b^{\chi_{c1}(3872)}/F_b^{\psi(2S)}$, are assigned as systematic uncertainty. The mean value of the t_z resolution function is fixed to zero in the reference fit. However, the reconstructed t_z distribution could be biased, for example due to tracks from b-hadron decays being included in the PV reconstruction. The mean value of the resolution function is left to vary freely and the difference of the $F_b^{\chi_{c1}(3872)}/F_b^{\psi(2S)}$ ratio is assigned as systematic uncertainty.

Table 1: Systematic uncertainties of the production cross-section of $\chi_{c1}(3872)$ relative to $\psi(2S)$ mesons in the kinematic region $4 < p_{\mathrm{T}} < 20$ GeV/c and $2.0 < y < 4.5$. Ranges are due to the variation across the (p_{T}, y) intervals. When only a range is given for the 13 TeV data it is shared between different data-taking years. The large ranges in some cases are due to statistical fluctuations of the signal or control samples used to evaluate the uncertainties.

Sources		Systematic uncertainty (%)			
		8 TeV	13 TeV		
		2012	2016	2017	2018
Mass fit	Signal lineshape	0.6		2.3	
	Fraction of two DSCBs	0.0–3.6		0.0–5.6	
	$\sigma_2^{\psi(2S)}/\sigma_1^{\psi(2S)}$	0.0–2.7		0.0–6.8	
	$\sigma_1^{\chi_{c1}(3872)}/\sigma_1^{\psi(2S)}$	0.2–3.6		0.2–5.1	
	$\sigma_2^{\chi_{c1}(3872)}/\sigma_2^{\psi(2S)}$	0.2–5.6		0.2–6.2	
	Background lineshape	0.0–1.5		0.0–3.7	
t_z fit	t_z resolution function	0.0–1.4	0.0–3.0	0.0–1.6	0.0–1.0
	Fixed mean of t_z resolution	0.0–0.4	0.0–1.0	0.0–0.8	0.0–0.6
	Wrong PV	0.0–2.8	0.0–4.1	0.0–3.6	0.0–1.8
	Backgrond shape	2.4		2.4	
	Fixed pseudolifetime	0.1–10.9	1.0–12.1	1.3–8.0	1.3–7.8
Tracking		0.1–0.7	0.1–0.2	0.1–1.4	0.1–1.0
Muon identification		0.0–6.1	0.0–1.8	0.0–1.8	0.0–1.5
Pion identification		0.1–6.7	0.0–0.4	0.0–0.9	0.0–0.3
Trigger thresholds		–	0.0–15.1	0.3–6.4	0.3–7.3
Simulation weighting		4.5–9.3	3.6–7.4	3.2–8.9	3.2–6.1
Global event requirements		0.5		1.9	
$M_{\pi^+\pi^-}$ spectrum		2.0		2.0	
Trigger efficiency		1.0		1.0	
Total systematic uncertainty		6.7–14.8	7.1–17.9	6.0–15.3	6.0–13.1
Total statistical uncertainty: prompt		7–17	5–19	6–31	5–13
Total statistical uncertainty: nonprompt		13–26	11–23	10–32	9–19

The long tail of the t_z distribution is due to misassociated primary vertices that can affect the fit result. Instead of using the different-event method, the tail is described with a bifurcated exponential with equal slope parameters on the positive and negative sides. The relative difference of $F_b^{\chi_{c1}(3872)}/F_b^{\psi(2S)}$ values between the two fits is used to assign the corresponding uncertainty. The t_z distribution for the background is obtained using the *sPlot* technique. The small correlation between $M_{J/\psi\pi^+\pi^-}$ and t_z affects the $F_b^{\chi_{c1}(3872)}/F_b^{\psi(2S)}$ by 2.4%, which is taken as systematic uncertainty. The pseudolifetime of nonprompt $\chi_{c1}(3872)$ candidates is fixed to 1.5 ps in the reference fit, which could affect the fitted F_b fraction. As an alternative, the $\chi_{c1}(3872)$ pseudolifetime is fixed to that of the $\psi(2S)$ contribution. The difference of $F_b^{\chi_{c1}(3872)}/F_b^{\psi(2S)}$ ratios between the reference and the alternative fits for each year is assigned as systematic uncertainty.

The track detection efficiencies are determined from a simulated sample in each (p_{T}, y) interval, and are corrected using control data. The statistical uncertainty due to the limited size of the control data sample is propagated using a large number of pseudoexperiments.

For each pseudoexperiment, a new efficiency-correction ratio as a function of the (p_{T}, y) interval is generated according to a Gaussian distribution where the original efficiency ratio and its uncertainty are used as the Gaussian mean and standard deviation, respectively.

The systematic uncertainty due to particle identification is studied considering the following contributions. The first is the statistical uncertainty due to the limited size of the calibration sample, which is estimated using pseudoexperiments and found to be negligible compared to other systematic uncertainties. The second is due to the binning scheme of the calibration sample. This contribution is studied by varying the binning in momentum, pseudorapidity and track multiplicity. The maximum differences among these contributions on the efficiency ratios are taken as systematic uncertainty.

The hardware-trigger thresholds on muon and hadron p_{T} varied throughout data taking, however only one value is used in the simulation. Differences in the trigger efficiencies observed when varying the thresholds in the simulation are taken as a source of systematic uncertainty. The p_{T} and y distributions of the simulated $\chi_{c1}(3872)$ and $\psi(2S)$ samples are corrected to match those in the data. The uncertainty on the simulation weighting is studied by propagating the statistical uncertainty on the correction using the Bootstrap method [34], where the root-mean-square of the resulting efficiency distribution is taken as systematic uncertainty. The effects of the global event requirements are estimated through the difference of the $\epsilon_{\psi(2S)}/\epsilon_{\chi_{c1}(3872)}$ ratio between the data and the simulation. The $M_{\pi^+\pi^-}$ distributions in the data and the simulation are slightly different, especially in the high $M_{\pi^+\pi^-}$ region. This difference affects the $\epsilon_{\psi(2S)}/\epsilon_{\chi_{c1}(3872)}$ ratio and is taken as systematic uncertainty. The systematic uncertainty on the trigger efficiency is taken from J/ψ pair production measurement [35].

6 Results and conclusion

The double-differential cross-section of the $\chi_{c1}(3872)$ state relative to that of the $\psi(2S)$ meson is measured as a function of p_{T} and y using pp collision data taken at centre-of-mass energies of $\sqrt{s} = 8$ and 13 TeV. The analysis assumes unpolarised production (a study on the impact of polarisation is described in Appendix A). For the per-year measurements at 13 TeV, the combination of the cross-section ratios is performed using the Best Linear Unbiased Estimate (BLUE) method [36–38]. The weighted average of these measurements is calculated by minimising the total uncertainty of the result and accounting for correlations between per-year measurements. The systematic uncertainties due to the $M_{J/\psi\pi^+\pi^-}$ and t_z fit are considered to be 100 % correlated, and the statistical and systematic uncertainties due to PID and tracking are considered to be uncorrelated. The cross-section ratios for promptly and nonpromptly produced mesons measured with the 8 and 13 TeV data samples as a function of p_{T} and y are shown in Figs. 3 and 4, respectively. The ratios, integrated over the kinematic region $4 < p_{\mathrm{T}} < 20$ GeV/c and $2.0 < y < 4.5$, are obtained to be

$$
\begin{aligned}
R^{8\,\mathrm{TeV}}_{\mathrm{prompt}} &= (7.6 \pm 0.5 \pm 0.9) \times 10^{-2}, \\
R^{8\,\mathrm{TeV}}_{\mathrm{nonprompt}} &= (4.6 \pm 0.4 \pm 0.5) \times 10^{-2}, \\
R^{13\,\mathrm{TeV}}_{\mathrm{prompt}} &= (7.6 \pm 0.3 \pm 0.6) \times 10^{-2}, \\
R^{13\,\mathrm{TeV}}_{\mathrm{nonprompt}} &= (4.4 \pm 0.2 \pm 0.4) \times 10^{-2},
\end{aligned}
$$

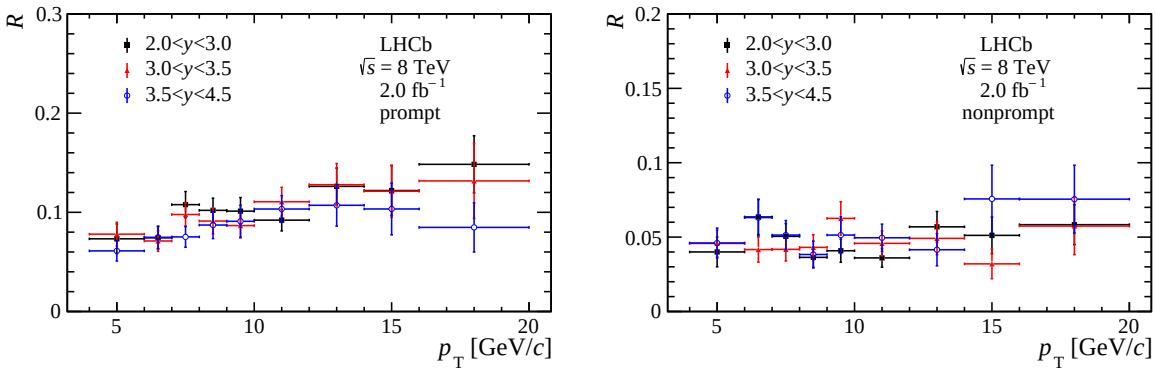

Figure 3: Ratios of differential cross-section times the branching ratio to the $J/\psi\pi^+\pi^-$ final state between $\chi_{c1}(3872)$ and $\psi(2S)$ mesons from (left) prompt production and (right) nonprompt from b-hadron decays, for the $\sqrt{s} = 8$ TeV sample as a function of $p_{\rm T}$ in intervals of rapidity. In all panels, the error bars represent the sum in quadrature of the statistical and systematic uncertainties.

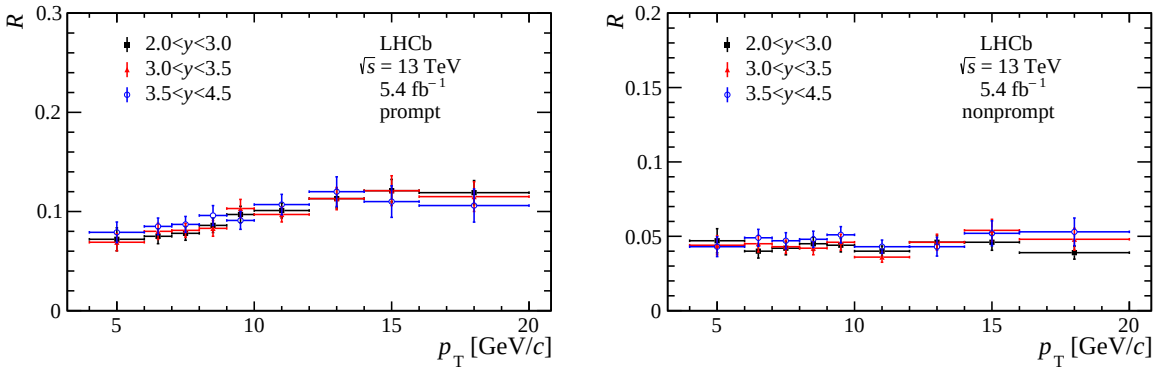

Figure 4: Ratios of differential cross-section times the branching ratio to the $J/\psi\pi^+\pi^-$ final state between $\chi_{c1}(3872)$ and $\psi(2S)$ mesons from (left) prompt production and (right) nonprompt from b-hadron decays, for the $\sqrt{s} = 13$ TeV sample as a function of $p_{\rm T}$ in intervals of rapidity. In all panels, the error bars represent the sum in quadrature of the statistical and systematic uncertainties.

where the first uncertainties are statistical and the second systematic.

The double ratio of the prompt $\chi_{c1}(3872)$ and $\psi(2S)$ production cross-sections between 13 and 8 TeV is also calculated using the measured cross-section ratio for 8 TeV and the combined ratio for 13 TeV. Figure 5 shows the double ratio of production cross-sections as a function of $p_{\rm T}$ integrated over the kinematic region $2.0 < y < 4.5$. A first-order polynomial of the form $R^{13\,\rm TeV}/R^{8\,\rm TeV} = a_0 + a_1 p_{\rm T}$ is used to fit the double ratio, yielding $a_0 = 0.99 \pm 0.23$ and a slope of $a_1 = (4 \pm 23) \times 10^{-3} (\,\text{GeV}/c)^{-1}$, consistent with zero.

In summary, the production cross-section of the $\chi_{c1}(3872)$ state relative to the $\psi(2S)$ meson is measured using pp data collected at centre-of-mass energies of 8 and 13 TeV. The double-differential cross-section ratio, as a function of $p_{\rm T}$ and y in the ranges $4 < p_{\rm T} < 20$ GeV/c and $2.0 < y < 4.5$, are determined for prompt and nonprompt production of $\chi_{c1}(3872)$ states relative to $\psi(2S)$ mesons. The prompt ratio increases as a function of $p_{\rm T}$, showing that the $\chi_{c1}(3872)$ production is enhanced relative to the one of prompt $\psi(2S)$ mesons in the higher $p_{\rm T}$ region. This behaviour is similar to the case of prompt production

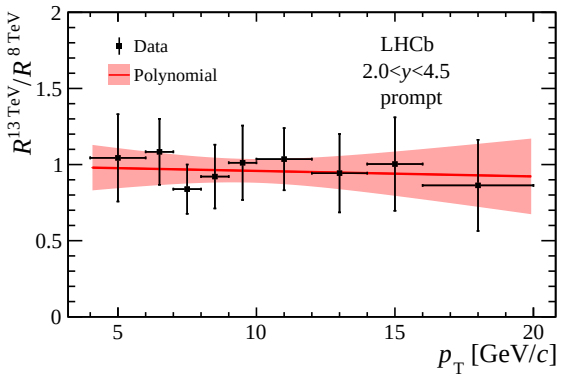

Figure 5: Double ratio of the prompt $\chi_{c1}(3872)$ production cross-section relative to that of $\psi(2S)$ mesons between 13 and 8 TeV as a function of p_{T} integrated over $2.0 < y < 4.5$. The red line with the solid band represent the fit result to a first-order polynomial and its uncertainty.

of $\psi(2S)$ relative to J/ψ mesons as measured by the CMS [39] and LHCb experiments [40], and is consistent with theoretical predictions [41]. Using the production cross-section of the $\psi(2S)$ meson measured by the LHCb experiment at 13 TeV [42], the absolute production cross-section of the $\chi_{c1}(3872)$ meson at 13 TeV multiplied by its branching fraction to the $J/\psi\pi^+\pi^-$ final state is determined as a function of p_{T}, as detailed in Appendix B. The result is found to agree in the $p_{\mathrm{T}} > 10\,\mathrm{GeV}/c$ region with NLO NRQCD predictions [12], which model the $\chi_{c1}(3872)$ state as a mixture of $\chi_{c1}(2P)$ and $D^0\overline{D}^{*0}$ molecule states, produced through its $\chi_{c1}(2P)$ component. The prompt cross-section ratios at 13 and 8 TeV are also compared, and no significant dependence on the centre-of-mass energy is found. The nonprompt ratio of cross-sections is consistent with a constant trend as a function of p_{T}, determined by the b-decay branching ratios.

Acknowledgements

We express our gratitude to our colleagues in the CERN accelerator departments for the excellent performance of the LHC. We thank the technical and administrative staff at the LHCb institutes. We acknowledge support from CERN and from the national agencies: CAPES, CNPq, FAPERJ and FINEP (Brazil); MOST and NSFC (China); CNRS/IN2P3 (France); BMBF, DFG and MPG (Germany); INFN (Italy); NWO (Netherlands); MNiSW and NCN (Poland); MEN/IFA (Romania); MSHE (Russia); MICINN (Spain); SNSF and SER (Switzerland); NASU (Ukraine); STFC (United Kingdom); DOE NP and NSF (USA). We acknowledge the computing resources that are provided by CERN, IN2P3 (France), KIT and DESY (Germany), INFN (Italy), SURF (Netherlands), PIC (Spain), GridPP (United Kingdom), RRCKI and Yandex LLC (Russia), CSCS (Switzerland), IFIN-HH (Romania), CBPF (Brazil), PL-GRID (Poland) and NERSC (USA). We are indebted to the communities behind the multiple open-source software packages on which we depend. Individual groups or members have received support from ARC and ARDC (Australia); AvH Foundation (Germany); EPLANET, Marie Skłodowska-Curie Actions and ERC (European Union); A*MIDEX, ANR, IPhU and Labex P2IO, and Région Auvergne-Rhône-Alpes (France); Key Research Program of Frontier Sciences of CAS, CAS PIFI, CAS CCEPP, Fundamental Research Funds for the Central Universities, and Sci.

& Tech. Program of Guangzhou (China); RFBR, RSF and Yandex LLC (Russia); GVA, XuntaGal and GENCAT (Spain); the Leverhulme Trust, the Royal Society and UKRI (United Kingdom).

Appendices

A Polarisation of $\psi(2S)$ and $\chi_{c1}(3872)$ mesons

The polarisation of the J/ψ meson is directly inherited from the $\psi(2S)$ parent, since the dipion system is produced in an S-wave state relative to the J/ψ meson. For the $\chi_{c1}(3872) \to J/\psi\pi^+\pi^-$ decay, the determination of the $\chi_{c1}(3872)$ polarisation can be obtained by measuring the dimuon angular decay distribution in the rest frame of the J/ψ daughter, as discussed in Refs. [43, 44]. The angular dependence of the $J/\psi \to \mu^+\mu^-$ decay for $\chi_{c1}(3872)$ and $\psi(2S)$ mesons is

$$\frac{d^2N}{d\cos\theta d\phi} \propto 1 + \lambda_\theta \cos^2\theta + \lambda_\phi \sin^2\theta \cos 2\phi + \lambda_{\theta\phi} \sin 2\theta \cos\phi \,, \tag{3}$$

where λ_i are the polarisation parameters and $\theta(\phi)$ are the polar (azimuthal) angles between the positively charged muon in the $J/\psi \to \mu^+\mu^-$ rest frame and the direction of the $\psi(2S)$ meson in the laboratory frame. Various polarisation hypotheses are considered:

- Unpolarised, with an isotropic distribution that is independent of the polarisation parameters, $\lambda_\theta = \lambda_\phi = \lambda_{\theta\phi} = 0$. This is used as the central hypothesis.
- Transversely polarised with $\lambda_\theta = +1, \lambda_\phi = \lambda_{\theta\phi} = 0$, labelled as T_{+0}.
- Transversely polarised with $\lambda_\theta = +1, \lambda_\phi = +1, \lambda_{\theta\phi} = 0$, labelled as T_{++}.
- Transversely polarised with $\lambda_\theta = +1, \lambda_\phi = -1, \lambda_{\theta\phi} = 0$, labelled as T_{+-}.
- Longitudinaly polarised, with the parameters $\lambda_\theta = -1, \lambda_\phi = \lambda_{\theta\phi} = 0$, labelled as L.
- Off-Plane Positive, with the polarisation parameters $\lambda_\theta = 0, \lambda_\phi = 0, \lambda_{\theta\phi} = +0.5$, labelled as $OP+$.
- Off-Plane Negative, with the polarisation parameters $\lambda_\theta = 0, \lambda_\phi = 0, \lambda_{\theta\phi} = -0.5$, labelled as $OP-$.

The acceptance weights are calculated for each of these scenarios in each (p_{T}, y) interval. The ratios of the acceptance efficiencies for each polarisation scenario to those of the unpolarised case are shown in Fig. 6 for $\psi(2S)$ mesons and Fig. 7 for the $\chi_{c1}(3872)$ state, and the values are listed in Tables 2, 3, and 4 for the former, and Tables 5, 6, and 7 for the latter.

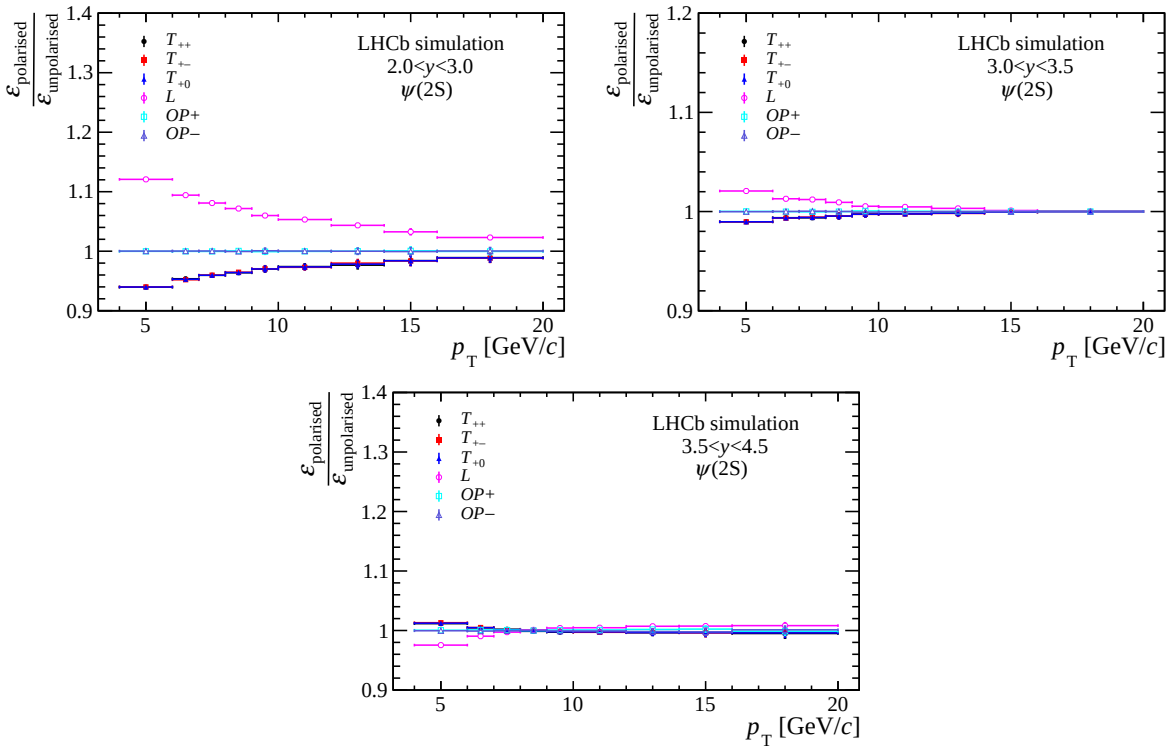

Figure 6: Ratio of acceptance efficiencies for $\psi(2S)$ mesons for various polarisation hypotheses with respect to the unpolarised case.

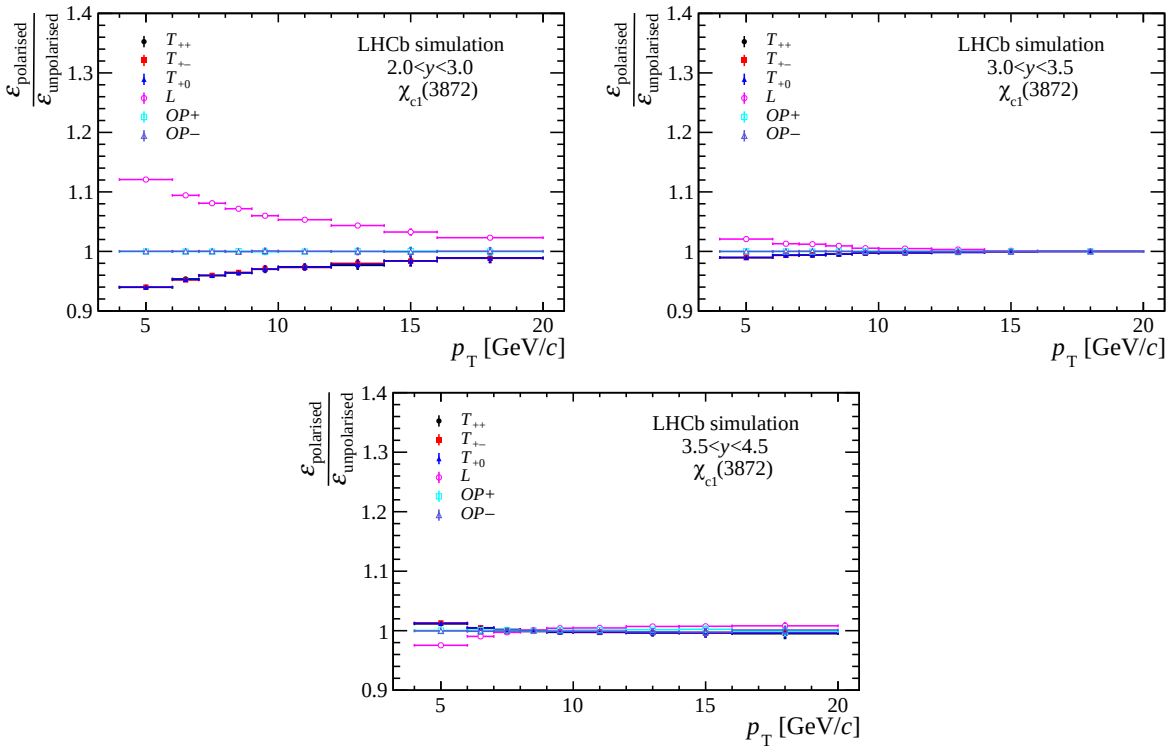

Figure 7: Ratio of acceptance efficiencies for $\chi_{c1}(3872)$ mesons for various polarisation hypotheses with respect to the unpolarised case.

Table 2: Ratio of acceptance efficiencies for $\psi(2S)$ mesons for various polarisation hypotheses with respect to the unpolarised case, in the interval $2.0 < y < 3.0$.

p_{T} [GeV/c]	T_{+0}	T_{++}	T_{+-}	L	$OP+$	$OP-$
4-6	0.940	0.940	0.940	1.121	1.000	1.000
6-7	0.953	0.954	0.952	1.094	1.000	1.000
7-8	0.960	0.959	0.960	1.081	1.000	1.000
8-9	0.964	0.964	0.965	1.072	1.000	1.000
9-10	0.970	0.970	0.970	1.060	0.999	1.001
10-12	0.974	0.974	0.973	1.053	1.000	1.000
12-14	0.978	0.977	0.980	1.043	1.000	1.000
14-16	0.984	0.984	0.984	1.033	1.001	0.999
16-20	0.989	0.989	0.988	1.023	1.000	1.000

Table 3: Ratio of acceptance efficiencies for $\psi(2S)$ mesons for various polarisation hypotheses with respect to the unpolarised case, in the interval $3.0 < y < 3.5$.

p_{T} [GeV/c]	T_{+0}	T_{++}	T_{+-}	L	$OP+$	$OP-$
4-6	0.990	0.990	0.990	1.021	1.000	1.000
6-7	0.994	0.994	0.993	1.013	1.000	1.000
7-8	0.994	0.994	0.994	1.012	1.000	1.000
8-9	0.995	0.995	0.996	1.009	1.000	1.000
9-10	0.997	0.997	0.997	1.005	1.001	0.999
10-12	0.998	0.998	0.998	1.005	1.000	1.000
12-14	0.998	0.999	0.998	1.003	1.000	1.000
14-16	1.000	1.000	0.999	1.001	1.000	1.000
16-20	1.000	1.000	1.000	1.000	1.000	1.000

Table 4: Ratio of acceptance efficiencies for $\psi(2S)$ mesons for various polarisation hypotheses with respect to the unpolarised case, in the interval $3.5 < y < 4.5$.

p_{T} [GeV/c]	T_{+0}	T_{++}	T_{+-}	L	$OP+$	$OP-$
4-6	1.012	1.012	1.013	0.975	1.000	1.000
6-7	1.005	1.005	1.005	0.990	1.001	0.999
7-8	1.001	1.002	1.001	0.997	1.001	0.999
8-9	0.999	0.999	1.000	1.001	1.000	1.000
9-10	0.998	0.997	0.999	1.004	1.001	0.999
10-12	0.998	0.998	0.997	1.005	1.001	0.999
12-14	0.996	0.996	0.997	1.007	1.002	0.998
14-16	0.996	0.997	0.996	1.007	1.002	0.998
16-20	0.996	0.995	0.997	1.008	0.999	1.001

Table 5: Ratio of acceptance efficiencies for $\chi_{c1}(3872)$ mesons for various polarisation hypotheses with respect to the unpolarised case, in the interval $2.0 < y < 3.0$.

p_{T} [GeV/c]	T_{+0}	T_{++}	T_{+-}	L	$OP+$	$OP-$
4-6	0.941	0.941	0.941	1.118	1.000	1.000
6-7	0.952	0.952	0.952	1.096	1.000	1.000
7-8	0.958	0.958	0.958	1.084	1.000	1.000
8-9	0.964	0.963	0.965	1.071	1.000	1.000
9-10	0.968	0.968	0.968	1.063	0.999	1.001
10-12	0.973	0.972	0.973	1.055	1.000	1.000
12-14	0.977	0.978	0.975	1.047	1.000	1.000
14-16	0.985	0.984	0.986	1.030	1.000	1.000
16-20	0.986	0.987	0.986	1.027	1.001	0.999

Table 6: Ratio of acceptance efficiencies for $\chi_{c1}(3872)$ mesons for various polarisation hypotheses with respect to the unpolarised case, in the interval $3.0 < y < 3.5$.

p_{T} [GeV/c]	T_{+0}	T_{++}	T_{+-}	L	$OP+$	$OP-$
4-6	0.990	0.990	0.990	1.021	1.000	1.000
6-7	0.992	0.992	0.993	1.015	1.000	1.000
7-8	0.994	0.994	0.995	1.012	1.000	1.000
8-9	0.995	0.995	0.996	1.009	1.000	1.000
9-10	0.997	0.998	0.997	1.005	0.999	1.001
10-12	0.997	0.997	0.998	1.005	1.000	1.000
12-14	0.999	0.999	0.999	1.002	1.000	1.000
14-16	0.998	0.998	0.998	1.003	1.000	1.000
16-20	0.999	0.999	0.999	1.002	1.001	0.999

Table 7: Ratio of acceptance efficiencies for $\chi_{c1}(3872)$ mesons for various polarisation hypotheses with respect to the unpolarised case, in the interval $3.5 < y < 4.5$.

p_{T} [GeV/c]	T_{+0}	T_{++}	T_{+-}	L	$OP+$	$OP-$
4-6	1.014	1.014	1.013	0.972	1.000	1.000
6-7	1.006	1.006	1.006	0.988	1.001	0.999
7-8	1.003	1.003	1.003	0.995	1.001	0.999
8-9	0.999	0.998	1.000	1.002	1.000	1.000
9-10	0.999	0.999	0.999	1.002	1.001	0.999
10-12	0.996	0.997	0.996	1.007	1.001	0.999
12-14	0.996	0.996	0.995	1.008	1.001	0.999
14-16	0.997	0.996	0.997	1.006	0.999	1.001
16-20	0.998	0.998	0.998	1.004	1.000	1.000

B Absolute cross-section of $\chi_{c1}(3872)$

As defined in Eq. (2), the absolute production cross-section of the $\chi_{c1}(3872)$ state times the branching fraction can be calculated using the measured cross-section ratio times $\sigma_{\psi(2S)}\mathcal{B}(\psi(2S)\to J/\psi\pi^+\pi^-)$. The value of $\sigma_{\psi(2S)}$ is taken from the $\psi(2S) \to \mu^+\mu^-$ analysis [42]. The world average for the $\psi(2S) \to J/\psi\pi^+\pi^-$ branching fraction is $\mathcal{B}(\psi(2S) \to J/\psi\pi^+\pi^-) = (34.68 \pm 0.30) \times 10^{-2}$ [31]. Figure 8 shows the measured cross-section times branching fractions as a function of $p_{\rm T}$ for prompt $\chi_{c1}(3872)$ mesons compared to NLO NRQCD predictions [12] and from b decays compared to FONLL predictions [45, 46]. The prompt $\chi_{c1}(3872)$ production in NLO NRQCD can be expressed as

$$d\sigma(pp \to \chi_{c1}(3872)) = d\sigma(pp \to \chi'_{c1}) \cdot k, \tag{4}$$

where $k = Z_{c\bar{c}} \cdot \mathcal{B}(\chi_{c1}(3872) \to J/\psi\pi^+\pi^-)$, the $Z_{c\bar{c}}$ is the probability of the χ'_{c1} component in the $\chi_{c1}(3872)$. The number of $k = 0.014 \pm 0.006$ is extracted by fitting the CMS data [10]. The prompt production is consistent with NLO NRQCD in the $p_{\rm T} > 10\,{\rm GeV}/c$ region. The same settings of FONLL as for $\psi(2S)$ mesons are used, except that $\mathcal{B}(b \to \chi_{c1}(3872))\mathcal{B}(\chi_{c1}(3872) \to J/\psi\pi^+\pi^-) = (4.3 \pm 0.5) \times 10^{-5}$ is taken from this analysis. The FONLL calculation is also consistent with the measurement. The absolute production cross-section can be derived from this result by using the recently measured $\mathcal{B}(\chi_{c1}(3872) \to J/\psi\pi^+\pi^-) = (4.1 \pm 1.3)\%$ [47] but the precision is insufficient to further improve the comparison with the various predictions.

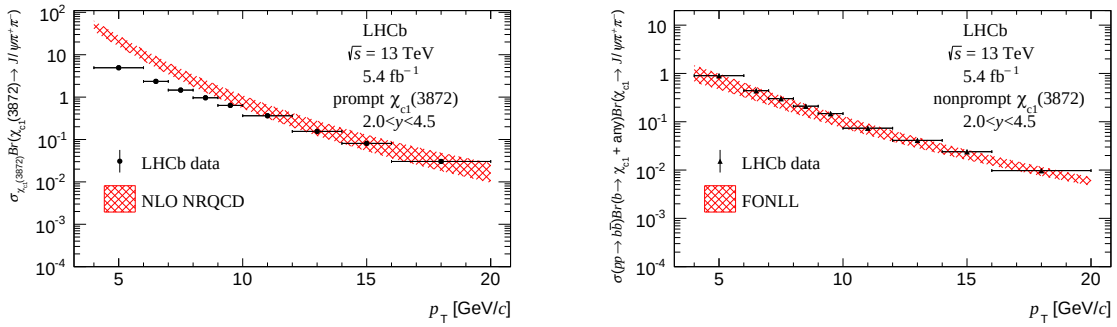

Figure 8: Measured production cross-section times branching fractions as a function of $p_{\rm T}$ for (left) prompt $\chi_{c1}(3872)$ mesons compared to NLO NRQCD predictions [12] and (right) from b decays compared to FONLL predictions [45, 46].

References

[1] Belle collaboration, S. K. Choi *et al.*, *Observation of a narrow charmonium-like state in exclusive $B^{\pm} \to K^{\pm}\pi^{+}\pi^{-}J/\psi$ decays*, Phys. Rev. Lett. **91** (2003) 262001, arXiv:hep-ex/0309032.

[2] BaBar collaboration, B. Aubert *et al.*, *Study of the $B \to J/\psi K^{-}\pi^{+}\pi^{-}$ decay and measurement of the $B \to X(3872)K^{-}$ branching fraction*, Phys. Rev. **D71** (2005) 071103, arXiv:hep-ex/0406022.

[3] CDF collaboration, D. Acosta *et al.*, *Observation of the narrow state $X(3872) \to J/\psi\pi^{+}\pi^{-}$ in $\bar{p}p$ collisions at $\sqrt{s} = 1.96$ TeV*, Phys. Rev. Lett. **93** (2004) 072001, arXiv:hep-ex/0312021.

[4] D0 collaboration, V. M. Abazov *et al.*, *Observation and properties of the $X(3872)$ decaying to $J/\psi\pi^{+}\pi^{-}$ in $p\bar{p}$ collisions at $\sqrt{s} = 1.96$ TeV*, Phys. Rev. Lett. **93** (2004) 162002, arXiv:hep-ex/0405004.

[5] LHCb collaboration, R. Aaij *et al.*, *Determination of the $X(3872)$ meson quantum numbers*, Phys. Rev. Lett. **110** (2013) 222001, arXiv:1302.6269.

[6] N. A. Tornqvist, *Isospin breaking of the narrow charmonium state of Belle at 3872-MeV as a deuson*, Phys. Lett. **B590** (2004) 209, arXiv:hep-ph/0402237.

[7] E. Braaten and M. Kusunoki, *Exclusive production of the X(3872) in B meson decay*, Phys. Rev. **D71** (2005) 074005, arXiv:hep-ph/0412268.

[8] LHCb collaboration, R. Aaij *et al.*, *Study of the line shape of the $\chi_{c1}(3872)$ state*, Phys. Rev. **D102** (2020) 092005, arXiv:2005.13419.

[9] LHCb collaboration, R. Aaij *et al.*, *Study of the $\psi_2(3823)$ and $\chi_{c1}(3872)$ states in $B^{+} \to (J/\psi\pi^{+}\pi^{-})K^{+}$ decays*, JHEP **08** (2020) 123, arXiv:2005.13422.

[10] CMS collaboration, S. Chatrchyan *et al.*, *Measurement of the X(3872) production cross-section via decays to $J/\psi\pi^{+}\pi^{-}$ in pp collisions at $\sqrt{s} = 7$ TeV*, JHEP **04** (2013) 154, arXiv:1302.3968.

[11] P. Artoisenet and E. Braaten, *Production of the X(3872) at the Tevatron and the LHC*, Phys. Rev. **D81** (2010) 114018, arXiv:0911.2016.

[12] C. Meng, H. Han, and K.-T. Chao, *X(3872) and its production at hadron colliders*, Phys. Rev. **D96** (2017) 074014, arXiv:1304.6710.

[13] ATLAS collaboration, M. Aaboud *et al.*, *Measurements of $\psi(2S)$ and $X(3872) \to J/\psi\pi^{+}\pi^{-}$ production in pp collisions at $\sqrt{s} = 8$ TeV with the ATLAS detector*, JHEP **01** (2017) 117, arXiv:1610.09303.

[14] LHCb collaboration, R. Aaij *et al.*, *Modification of $\chi_{c1}(3872)$ and $\psi(2S)$ production in pp collisions at $\sqrt{s} = 8$ TeV*, Phys. Rev. Lett. **126** (2021) 092001, arXiv:2009.06619.

[15] A. Esposito *et al.*, *The nature of $X(3872)$ from high-multiplicity pp collisions*, Eur. Phys. J. **C81** (2021) 669, arXiv:2006.15044.

[16] E. Braaten, L.-P. He, K. Ingles, and J. Jiang, *Production of $X(3872)$ at high multiplicity*, Phys. Rev. **D103** (2021) L071901, arXiv:2012.13499.

[17] LHCb collaboration, R. Aaij *et al.*, *Observation of $X(3872)$ production in pp collisions at $\sqrt{s} = 7$ TeV*, Eur. Phys. J. **C72** (2012) 1972, arXiv:1112.5310.

[18] LHCb collaboration, A. A. Alves Jr. *et al.*, *The LHCb detector at the LHC*, JINST **3** (2008) S08005.

[19] LHCb collaboration, R. Aaij *et al.*, *LHCb detector performance*, Int. J. Mod. Phys. **A30** (2015) 1530022, arXiv:1412.6352.

[20] R. Aaij *et al.*, *Performance of the LHCb Vertex Locator*, JINST **9** (2014) P09007, arXiv:1405.7808.

[21] R. Arink *et al.*, *Performance of the LHCb Outer Tracker*, JINST **9** (2014) P01002, arXiv:1311.3893.

[22] P. d'Argent *et al.*, *Improved performance of the LHCb Outer Tracker in LHC Run 2*, JINST **12** (2017) P11016, arXiv:1708.00819.

[23] M. Adinolfi *et al.*, *Performance of the LHCb RICH detector at the LHC*, Eur. Phys. J. **C73** (2013) 2431, arXiv:1211.6759.

[24] R. Aaij *et al.*, *The LHCb trigger and its performance in 2011*, JINST **8** (2013) P04022, arXiv:1211.3055.

[25] T. Sjöstrand, S. Mrenna, and P. Skands, *A brief introduction to PYTHIA 8.1*, Comput. Phys. Commun. **178** (2008) 852, arXiv:0710.3820; T. Sjöstrand, S. Mrenna, and P. Skands, *PYTHIA 6.4 physics and manual*, JHEP **05** (2006) 026, arXiv:hep-ph/0603175.

[26] I. Belyaev *et al.*, *Handling of the generation of primary events in Gauss, the LHCb simulation framework*, J. Phys. Conf. Ser. **331** (2011) 032047.

[27] D. J. Lange, *The EvtGen particle decay simulation package*, Nucl. Instrum. Meth. **A462** (2001) 152.

[28] N. Davidson, T. Przedzinski, and Z. Was, *PHOTOS interface in C++: Technical and physics documentation*, Comp. Phys. Comm. **199** (2016) 86, arXiv:1011.0937.

[29] Geant4 collaboration, J. Allison *et al.*, *Geant4 developments and applications*, IEEE Trans. Nucl. Sci. **53** (2006) 270; Geant4 collaboration, S. Agostinelli *et al.*, *Geant4: A simulation toolkit*, Nucl. Instrum. Meth. **A506** (2003) 250.

[30] M. Clemencic *et al.*, *The LHCb simulation application, Gauss: Design, evolution and experience*, J. Phys. Conf. Ser. **331** (2011) 032023.

[31] Particle Data Group, P. A. Zyla *et al.*, *Review of particle physics*, Prog. Theor. Exp. Phys. **2020** (2020) 083C01.

[32] T. Skwarnicki, *A study of the radiative cascade transitions between the Upsilon-prime and Upsilon resonances*, PhD thesis, Institute of Nuclear Physics, Krakow, 1986, DESY-F31-86-02.

[33] M. Pivk and F. R. Le Diberder, *sPlot: A statistical tool to unfold data distributions*, Nucl. Instrum. Meth. **A555** (2005) 356, arXiv:physics/0402083.

[34] B. Efron, *The jackknife, the bootstrap and other resampling plans*, SIAM, 1982.

[35] LHCb collaboration, R. Aaij *et al.*, *Measurement of the J/ψ pair production cross-section in pp collisions at $\sqrt{s}$ =13 TeV*, JHEP **06** (2017) 047, Erratum ibid. **10** (2017) 068, arXiv:1612.07451.

[36] L. Lyons, D. Gibaut, and P. Clifford, *How to combine correlated estimates of a single physical quantity*, Nucl. Instrum. Meth. **A270** (1988) 110.

[37] A. Valassi, *Combining correlated measurements of several different physical quantities*, Nucl. Instrum. Meth. **A500** (2003) 391.

[38] A. Valassi and R. Chierici, *Information and treatment of unknown correlations in the combination of measurements using the BLUE method*, Eur. Phys. J. **C74** (2014) 2717, arXiv:1307.4003.

[39] CMS collaboration, S. Chatrchyan *et al.*, *J/ψ and $\psi(2S)$ production in pp collisions at $\sqrt{s} = 7$ TeV*, JHEP **02** (2012) 011, arXiv:1111.1557.

[40] LHCb collaboration, R. Aaij *et al.*, *Measurement of $\psi(2S)$ meson production in pp collisions at $\sqrt{s}$ =7 TeV*, Eur. Phys. J. **C72** (2012) 2100, Erratum ibid. **C80** (2020) 49, arXiv:1204.1258.

[41] V. A. Khoze, A. D. Martin, M. G. Ryskin, and W. J. Stirling, *Inelastic J/ψ and Υ hadroproduction*, Eur. Phys. J. **C39** (2005) 163, arXiv:hep-ph/0410020.

[42] LHCb collaboration, R. Aaij *et al.*, *Measurement of $\psi(2S)$ production cross-sections in proton-proton collisions at $\sqrt{s}$ =7 and 13 TeV*, Eur. Phys. J. **C80** (2020) 185, arXiv:1908.03099.

[43] CMS collaboration, A. M. Sirunyan *et al.*, *Constraints on the χ_{c1} versus χ_{c2} polarisations in proton-proton collisions at $\sqrt{s}$ = 8 TeV*, Phys. Rev. Lett. **124** (2020) 162002, arXiv:1912.07706.

[44] P. Faccioli, C. Lourenço, J. Seixas, and H. K. Wohri, *Determination of χ_c and χ_b polarizations from dilepton angular distributions in radiative decays*, Phys. Rev. **D83** (2011) 096001, arXiv:1103.4882.

[45] M. Cacciari, M. Greco, and P. Nason, *The $p_{\rm T}$ spectrum in heavy flavor hadroproduction*, JHEP **9805** (1998) 007, arXiv:hep-ph/9803400.

[46] M. Cacciari, M. L. Mangano, and P. Nason, *Gluon PDF constraints from the ratio of forward heavy-quark production at the LHC at $\sqrt{s} = 7$ and 13 TeV*, Eur. Phys. J. **C75** (2015) 610, arXiv:1507.06197.

[47] BaBar collaboration, J. P. Lees *et al.*, *Measurements of the absolute branching fractions of* $B^{\pm} \to K^{\pm} X_{c\bar{c}}$, Phys. Rev. Lett. **124** (2020) 152001, arXiv:1911.11740.

LHCb collaboration

R. Aaij[32], A.S.W. Abdelmotteleb[56], C. Abellán Beteta[50], F.J. Abudinen Gallego[56], T. Ackernley[60], B. Adeva[46], M. Adinolfi[54], H. Afsharnia[9], C. Agapopoulou[13], C.A. Aidala[87], S. Aiola[25], Z. Ajaltouni[9], S. Akar[65], J. Albrecht[15], F. Alessio[48], M. Alexander[59], A. Alfonso Albero[45], Z. Aliouche[62], G. Alkhazov[38], P. Alvarez Cartelle[55], S. Amato[2], J.L. Amey[54], Y. Amhis[11], L. An[48], L. Anderlini[22], A. Andreianov[38], M. Andreotti[21], F. Archilli[17], A. Artamonov[44], M. Artuso[68], K. Arzymatov[42], E. Aslanides[10], M. Atzeni[50], B. Audurier[12], S. Bachmann[17], M. Bachmayer[49], J.J. Back[56], P. Baladron Rodriguez[46], V. Balagura[12], W. Baldini[21], J. Baptista Leite[1], M. Barbetti[22], R.J. Barlow[62], S. Barsuk[11], W. Barter[61], M. Bartolini[24,h], F. Baryshnikov[83], J.M. Basels[14], S. Bashir[34], G. Bassi[29], B. Batsukh[68], A. Battig[15], A. Bay[49], A. Beck[56], M. Becker[15], F. Bedeschi[29], I. Bediaga[1], A. Beiter[68], V. Belavin[42], S. Belin[27], V. Bellee[50], K. Belous[44], I. Belov[40], I. Belyaev[41], G. Bencivenni[23], E. Ben-Haim[13], A. Berezhnoy[40], R. Bernet[50], D. Berninghoff[17], H.C. Bernstein[68], C. Bertella[48], A. Bertolin[28], C. Betancourt[50], F. Betti[48], Ia. Bezshyiko[50], S. Bhasin[54], J. Bhom[35], L. Bian[73], M.S. Bieker[15], S. Bifani[53], P. Billoir[13], M. Birch[61], F.C.R. Bishop[55], A. Bitadze[62], A. Bizzeti[22,k], M. Bjørn[63], M.P. Blago[48], T. Blake[56], F. Blanc[49], S. Blusk[68], D. Bobulska[59], J.A. Boelhauve[15], O. Boente Garcia[46], T. Boettcher[65], A. Boldyrev[82], A. Bondar[43], N. Bondar[38,48], S. Borghi[62], M. Borisyak[42], M. Borsato[17], J.T. Borsuk[35], S.A. Bouchiba[49], T.J.V. Bowcock[60], A. Boyer[48], C. Bozzi[21], M.J. Bradley[61], S. Braun[66], A. Brea Rodriguez[46], M. Brodski[48], J. Brodzicka[35], A. Brossa Gonzalo[56], D. Brundu[27], A. Buonaura[50], L. Buonincontri[28], A.T. Burke[62], C. Burr[48], A. Bursche[72], A. Butkevich[39], J.S. Butter[32], J. Buytaert[48], W. Byczynski[48], S. Cadeddu[27], H. Cai[73], R. Calabrese[21,f], L. Calefice[15,13], L. Calero Diaz[23], S. Cali[23], R. Calladine[53], M. Calvi[26,j], M. Calvo Gomez[85], P. Camargo Magalhaes[54], P. Campana[23], A.F. Campoverde Quezada[6], S. Capelli[26,j], L. Capriotti[20,d], A. Carbone[20,d], G. Carboni[31], R. Cardinale[24,h], A. Cardini[27], I. Carli[4], P. Carniti[26,j], L. Carus[14], K. Carvalho Akiba[32], A. Casais Vidal[46], G. Casse[60], M. Cattaneo[48], G. Cavallero[48], S. Celani[49], J. Cerasoli[10], D. Cervenkov[63], A.J. Chadwick[60], M.G. Chapman[54], M. Charles[13], Ph. Charpentier[48], G. Chatzikonstantinidis[53], C.A. Chavez Barajas[60], M. Chefdeville[8], C. Chen[3], S. Chen[4], A. Chernov[35], V. Chobanova[46], S. Cholak[49], M. Chrzaszcz[35], A. Chubykin[38], V. Chulikov[38], P. Ciambrone[23], M.F. Cicala[56], X. Cid Vidal[46], G. Ciezarek[48], P.E.L. Clarke[58], M. Clemencic[48], H.V. Cliff[55], J. Closier[48], J.L. Cobbledick[62], V. Coco[48], J.A.B. Coelho[11], J. Cogan[10], E. Cogneras[9], L. Cojocariu[37], P. Collins[48], T. Colombo[48], L. Congedo[19,c], A. Contu[27], N. Cooke[53], G. Coombs[59], I. Corredoira [46], G. Corti[48], C.M. Costa Sobral[56], B. Couturier[48], D.C. Craik[64], J. Crkovská[67], M. Cruz Torres[1], R. Currie[58], C.L. Da Silva[67], S. Dadabaev[83], L. Dai[71], E. Dall'Occo[15], J. Dalseno[46], C. D'Ambrosio[48], A. Danilina[41], P. d'Argent[48], J.E. Davies[62], A. Davis[62], O. De Aguiar Francisco[62], K. De Bruyn[79], S. De Capua[62], M. De Cian[49], J.M. De Miranda[1], L. De Paula[2], M. De Serio[19,c], D. De Simone[50], P. De Simone[23], J.A. de Vries[80], C.T. Dean[67], D. Decamp[8], V. Dedu[10], L. Del Buono[13], B. Delaney[55], H.-P. Dembinski[15], A. Dendek[34], V. Denysenko[50], D. Derkach[82], O. Deschamps[9], F. Desse[11], F. Dettori[27,e], B. Dey[77], A. Di Cicco[23], P. Di Nezza[23], S. Didenko[83], L. Dieste Maronas[46], H. Dijkstra[48], V. Dobishuk[52], C. Dong[3], A.M. Donohoe[18], F. Dordei[27], A.C. dos Reis[1], L. Douglas[59], A. Dovbnya[51], A.G. Downes[8], M.W. Dudek[35], L. Dufour[48], V. Duk[78], P. Durante[48], J.M. Durham[67], D. Dutta[62], A. Dziurda[35], A. Dzyuba[38], S. Easo[57], U. Egede[69], V. Egorychev[41], S. Eidelman[43,v], S. Eisenhardt[58], S. Ek-In[49], L. Eklund[59,86], S. Ely[68], A. Ene[37], E. Epple[67], S. Escher[14], J. Eschle[50], S. Esen[13], T. Evans[48], A. Falabella[20], J. Fan[3], Y. Fan[6], B. Fang[73], S. Farry[60], D. Fazzini[26,j], M. Féo[48], A. Fernandez Prieto[46], A.D. Fernez[66], F. Ferrari[20,d], L. Ferreira Lopes[49], F. Ferreira Rodrigues[2], S. Ferreres Sole[32], M. Ferrillo[50], M. Ferro-Luzzi[48], S. Filippov[39], R.A. Fini[19], M. Fiorini[21,f], M. Firlej[34], K.M. Fischer[63], D.S. Fitzgerald[87],

C. Fitzpatrick[62], T. Fiutowski[34], A. Fkiaras[48], F. Fleuret[12], M. Fontana[13], F. Fontanelli[24,h], R. Forty[48], D. Foulds-Holt[55], V. Franco Lima[60], M. Franco Sevilla[66], M. Frank[48], E. Franzoso[21], G. Frau[17], C. Frei[48], D.A. Friday[59], J. Fu[6], Q. Fuehring[15], E. Gabriel[32], A. Gallas Torreira[46], D. Galli[20,d], S. Gambetta[58,48], Y. Gan[3], M. Gandelman[2], P. Gandini[25], Y. Gao[5], M. Garau[27], L.M. Garcia Martin[56], P. Garcia Moreno[45], J. García Pardiñas[26,j], B. Garcia Plana[46], F.A. Garcia Rosales[12], L. Garrido[45], C. Gaspar[48], R.E. Geertsema[32], D. Gerick[17], L.L. Gerken[15], E. Gersabeck[62], M. Gersabeck[62], T. Gershon[56], D. Gerstel[10], Ph. Ghez[8], L. Giambastiani[28], V. Gibson[55], H.K. Giemza[36], A.L. Gilman[63], M. Giovannetti[23,p], A. Gioventù[46], P. Gironella Gironell[45], L. Giubega[37], C. Giugliano[21,f,48], K. Gizdov[58], E.L. Gkougkousis[48], V.V. Gligorov[13], C. Göbel[70], E. Golobardes[85], D. Golubkov[41], A. Golutvin[61,83], A. Gomes[1,a], S. Gomez Fernandez[45], F. Goncalves Abrantes[63], M. Goncerz[35], G. Gong[3], P. Gorbounov[41], I.V. Gorelov[40], C. Gotti[26], E. Govorkova[48], J.P. Grabowski[17], T. Grammatico[13], L.A. Granado Cardoso[48], E. Graugés[45], E. Graverini[49], G. Graziani[22], A. Grecu[37], L.M. Greeven[32], N.A. Grieser[4], L. Grillo[62], S. Gromov[83], B.R. Gruberg Cazon[63], C. Gu[3], M. Guarise[21], M. Guittiere[11], P. A. Günther[17], E. Gushchin[39], A. Guth[14], Y. Guz[44], T. Gys[48], T. Hadavizadeh[69], G. Haefeli[49], C. Haen[48], J. Haimberger[48], T. Halewood-leagas[60], P.M. Hamilton[66], J.P. Hammerich[60], Q. Han[7], X. Han[17], T.H. Hancock[63], S. Hansmann-Menzemer[17], N. Harnew[63], T. Harrison[60], C. Hasse[48], M. Hatch[48], J. He[6,b], M. Hecker[61], K. Heijhoff[32], K. Heinicke[15], A.M. Hennequin[48], K. Hennessy[60], L. Henry[48], J. Heuel[14], A. Hicheur[2], D. Hill[49], M. Hilton[62], S.E. Hollitt[15], R. Hou[7], Y. Hou[6], J. Hu[17], J. Hu[72], W. Hu[7], X. Hu[3], W. Huang[6], X. Huang[73], W. Hulsbergen[32], R.J. Hunter[56], M. Hushchyn[82], D. Hutchcroft[60], D. Hynds[32], P. Ibis[15], M. Idzik[34], D. Ilin[38], P. Ilten[65], A. Inglessi[38], A. Ishteev[83], K. Ivshin[38], R. Jacobsson[48], H. Jage[14], S. Jakobsen[48], E. Jans[32], B.K. Jashal[47], A. Jawahery[66], V. Jevtic[15], F. Jiang[3], M. John[63], D. Johnson[48], C.R. Jones[55], T.P. Jones[56], B. Jost[48], N. Jurik[48], S.H. Kalavan Kadavath[34], S. Kandybei[51], Y. Kang[3], M. Karacson[48], M. Karpov[82], F. Keizer[48], D.M. Keller[68], M. Kenzie[56], T. Ketel[33], B. Khanji[15], A. Kharisova[84], S. Kholodenko[44], T. Kirn[14], V.S. Kirsebom[49], O. Kitouni[64], S. Klaver[32], N. Kleijne[29], K. Klimaszewski[36], M.R. Kmiec[36], S. Koliiev[52], A. Kondybayeva[83], A. Konoplyannikov[41], P. Kopciewicz[34], R. Kopecna[17], P. Koppenburg[32], M. Korolev[40], I. Kostiuk[32,52], O. Kot[52], S. Kotriakhova[21,38], P. Kravchenko[38], L. Kravchuk[39], R.D. Krawczyk[48], M. Kreps[56], F. Kress[61], S. Kretzschmar[14], P. Krokovny[43,v], W. Krupa[34], W. Krzemien[36], W. Kucewicz[35,t], M. Kucharczyk[35], V. Kudryavtsev[43,v], H.S. Kuindersma[32,33], G.J. Kunde[67], T. Kvaratskheliya[41], D. Lacarrere[48], G. Lafferty[62], A. Lai[27], A. Lampis[27], D. Lancierini[50], J.J. Lane[62], R. Lane[54], G. Lanfranchi[23], C. Langenbruch[14], J. Langer[15], O. Lantwin[83], T. Latham[56], F. Lazzari[29,q], R. Le Gac[10], S.H. Lee[87], R. Lefèvre[9], A. Leflat[40], S. Legotin[83], O. Leroy[10], T. Lesiak[35], B. Leverington[17], H. Li[72], P. Li[17], S. Li[7], Y. Li[4], Y. Li[4], Z. Li[68], X. Liang[68], T. Lin[61], R. Lindner[48], V. Lisovskyi[15], R. Litvinov[27], G. Liu[72], H. Liu[6], Q. Liu[6], S. Liu[4], A. Lobo Salvia[45], A. Loi[27], J. Lomba Castro[46], I. Longstaff[59], J.H. Lopes[2], S. Lopez Solino[46], G.H. Lovell[55], Y. Lu[4], C. Lucarelli[22], D. Lucchesi[28,l], S. Luchuk[39], M. Lucio Martinez[32], V. Lukashenko[32,52], Y. Luo[3], A. Lupato[62], E. Luppi[21,f], O. Lupton[56], A. Lusiani[29,m], X. Lyu[6], L. Ma[4], R. Ma[6], S. Maccolini[20,d], F. Machefert[11], F. Maciuc[37], V. Macko[49], P. Mackowiak[15], S. Maddrell-Mander[54], O. Madejczyk[34], L.R. Madhan Mohan[54], O. Maev[38], A. Maevskiy[82], D. Maisuzenko[38], M.W. Majewski[34], J.J. Malczewski[35], S. Malde[63], B. Malecki[48], A. Malinin[81], T. Maltsev[43,v], H. Malygina[17], G. Manca[27,e], G. Mancinelli[10], D. Manuzzi[20,d], D. Marangotto[25,i], J. Maratas[9,s], J.F. Marchand[8], U. Marconi[20], S. Mariani[22,g], C. Marin Benito[48], M. Marinangeli[49], J. Marks[17], A.M. Marshall[54], P.J. Marshall[60], G. Martelli[78], G. Martellotti[30], L. Martinazzoli[48,j], M. Martinelli[26,j], D. Martinez Santos[46], F. Martinez Vidal[47], A. Massafferri[1], M. Materok[14], R. Matev[48], A. Mathad[50], Z. Mathe[48], V. Matiunin[41], C. Matteuzzi[26], K.R. Mattioli[87], A. Mauri[32], E. Maurice[12], J. Mauricio[45], M. Mazurek[48], M. McCann[61], L. Mcconnell[18], T.H. Mcgrath[62], N.T. Mchugh[59], A. McNab[62],

R. McNulty[18], J.V. Mead[60], B. Meadows[65], G. Meier[15], N. Meinert[76], D. Melnychuk[36], S. Meloni[26,j], M. Merk[32,80], A. Merli[25,i], L. Meyer Garcia[2], M. Mikhasenko[48], D.A. Milanes[74], E. Millard[56], M. Milovanovic[48], M.-N. Minard[8], A. Minotti[26,j], L. Minzoni[21,f], S.E. Mitchell[58], B. Mitreska[62], D.S. Mitzel[48], A. Mödden [15], R.A. Mohammed[63], R.D. Moise[61], S. Mokhnenko[82], T. Mombächer[46], I.A. Monroy[74], S. Monteil[9], M. Morandin[28], G. Morello[23], M.J. Morello[29,m], J. Moron[34], A.B. Morris[75], A.G. Morris[56], R. Mountain[68], H. Mu[3], F. Muheim[58,48], M. Mulder[48], D. Müller[48], K. Müller[50], C.H. Murphy[63], D. Murray[62], P. Muzzetto[27,48], P. Naik[54], T. Nakada[49], R. Nandakumar[57], T. Nanut[49], I. Nasteva[2], M. Needham[58], I. Neri[21], N. Neri[25,i], S. Neubert[75], N. Neufeld[48], R. Newcombe[61], T.D. Nguyen[49], C. Nguyen-Mau[49,w], E.M. Niel[11], S. Nieswand[14], N. Nikitin[40], N.S. Nolte[64], C. Normand[8], C. Nunez[87], A. Oblakowska-Mucha[34], V. Obraztsov[44], T. Oeser[14], D.P. O'Hanlon[54], S. Okamura[21], R. Oldeman[27,e], F. Oliva[58], M.E. Olivares[68], C.J.G. Onderwater[79], R.H. O'Neil[58], A. Ossowska[35], J.M. Otalora Goicochea[2], T. Ovsiannikova[41], P. Owen[50], A. Oyanguren[47], K.O. Padeken[75], B. Pagare[56], P.R. Pais[48], T. Pajero[63], A. Palano[19], M. Palutan[23], Y. Pan[62], G. Panshin[84], A. Papanestis[57], M. Pappagallo[19,c], L.L. Pappalardo[21,f], C. Pappenheimer[65], W. Parker[66], C. Parkes[62], B. Passalacqua[21], G. Passaleva[22], A. Pastore[19], M. Patel[61], C. Patrignani[20,d], C.J. Pawley[80], A. Pearce[48], A. Pellegrino[32], M. Pepe Altarelli[48], S. Perazzini[20], D. Pereima[41], A. Pereiro Castro[46], P. Perret[9], M. Petric[59,48], K. Petridis[54], A. Petrolini[24,h], A. Petrov[81], S. Petrucci[58], M. Petruzzo[25], T.T.H. Pham[68], A. Philippov[42], L. Pica[29,m], M. Piccini[78], B. Pietrzyk[8], G. Pietrzyk[49], M. Pili[63], D. Pinci[30], F. Pisani[48], M. Pizzichemi[26,48,j], Resmi P.K[10], V. Placinta[37], J. Plews[53], M. Plo Casasus[46], F. Polci[13], M. Poli Lener[23], M. Poliakova[68], A. Poluektov[10], N. Polukhina[83,u], I. Polyakov[68], E. Polycarpo[2], S. Ponce[48], D. Popov[6,48], S. Popov[42], S. Poslavskii[44], K. Prasanth[35], L. Promberger[48], C. Prouve[46], V. Pugatch[52], V. Puill[11], H. Pullen[63], G. Punzi[29,n], H. Qi[3], W. Qian[6], J. Qin[6], N. Qin[3], R. Quagliani[49], B. Quintana[8], N.V. Raab[18], R.I. Rabadan Trejo[6], B. Rachwal[34], J.H. Rademacker[54], M. Rama[29], M. Ramos Pernas[56], M.S. Rangel[2], F. Ratnikov[42,82], G. Raven[33], M. Reboud[8], F. Redi[49], F. Reiss[62], C. Remon Alepuz[47], Z. Ren[3], V. Renaudin[63], R. Ribatti[29], S. Ricciardi[57], K. Rinnert[60], P. Robbe[11], G. Robertson[58], A.B. Rodrigues[49], E. Rodrigues[60], J.A. Rodriguez Lopez[74], E.R.R. Rodriguez Rodriguez[46], A. Rollings[63], P. Roloff[48], V. Romanovskiy[44], M. Romero Lamas[46], A. Romero Vidal[46], J.D. Roth[87], M. Rotondo[23], M.S. Rudolph[68], T. Ruf[48], R.A. Ruiz Fernandez[46], J. Ruiz Vidal[47], A. Ryzhikov[82], J. Ryzka[34], J.J. Saborido Silva[46], N. Sagidova[38], N. Sahoo[56], B. Saitta[27,e], M. Salomoni[48], C. Sanchez Gras[32], R. Santacesaria[30], C. Santamarina Rios[46], M. Santimaria[23], E. Santovetti[31,p], D. Saranin[83], G. Sarpis[14], M. Sarpis[75], A. Sarti[30], C. Satriano[30,o], A. Satta[31], M. Saur[15], D. Savrina[41,40], H. Sazak[9], L.G. Scantlebury Smead[63], A. Scarabotto[13], S. Schael[14], S. Scherl[60], M. Schiller[59], H. Schindler[48], M. Schmelling[16], B. Schmidt[48], S. Schmitt[14], O. Schneider[49], A. Schopper[48], M. Schubiger[32], S. Schulte[49], M.H. Schune[11], R. Schwemmer[48], B. Sciascia[23,48], S. Sellam[46], A. Semennikov[41], M. Senghi Soares[33], A. Sergi[24,h], N. Serra[50], L. Sestini[28], A. Seuthe[15], Y. Shang[5], D.M. Shangase[87], M. Shapkin[44], I. Shchemerov[83], L. Shchutska[49], T. Shears[60], L. Shekhtman[43,v], Z. Shen[5], V. Shevchenko[81], E.B. Shields[26,j], Y. Shimizu[11], E. Shmanin[83], J.D. Shupperd[68], B.G. Siddi[21], R. Silva Coutinho[50], G. Simi[28], S. Simone[19,c], N. Skidmore[62], T. Skwarnicki[68], M.W. Slater[53], I. Slazyk[21,f], J.C. Smallwood[63], J.G. Smeaton[55], A. Smetkina[41], E. Smith[50], M. Smith[61], A. Snoch[32], M. Soares[20], L. Soares Lavra[9], M.D. Sokoloff[65], F.J.P. Soler[59], A. Solovev[38], I. Solovyev[38], F.L. Souza De Almeida[2], B. Souza De Paula[2], B. Spaan[15], E. Spadaro Norella[25,i], P. Spradlin[59], F. Stagni[48], M. Stahl[65], S. Stahl[48], S. Stanislaus[63], O. Steinkamp[50,83], O. Stenyakin[44], H. Stevens[15], S. Stone[68], M. Straticiuc[37], D. Strekalina[83], F. Suljik[63], J. Sun[27], L. Sun[73], Y. Sun[66], P. Svihra[62], P.N. Swallow[53], K. Swientek[34], A. Szabelski[36], T. Szumlak[34], M. Szymanski[48], S. Taneja[62], A.R. Tanner[54], M.D. Tat[63], A. Terentev[83], F. Teubert[48], E. Thomas[48], D.J.D. Thompson[53], K.A. Thomson[60], V. Tisserand[9], S. T'Jampens[8], M. Tobin[4],

L. Tomassetti[21,f], X. Tong[5], D. Torres Machado[1], D.Y. Tou[13], M.T. Tran[49], E. Trifonova[83], C. Trippl[49], G. Tuci[6], A. Tully[49], N. Tuning[32,48], A. Ukleja[36], D.J. Unverzagt[17], E. Ursov[83], A. Usachov[32], A. Ustyuzhanin[42,82], U. Uwer[17], A. Vagner[84], V. Vagnoni[20], A. Valassi[48], G. Valenti[20], N. Valls Canudas[85], M. van Beuzekom[32], M. Van Dijk[49], E. van Herwijnen[83], C.B. Van Hulse[18], M. van Veghel[79], R. Vazquez Gomez[45], P. Vazquez Regueiro[46], C. Vázquez Sierra[48], S. Vecchi[21], J.J. Velthuis[54], M. Veltri[22,r], A. Venkateswaran[68], M. Veronesi[32], M. Vesterinen[56], D. Vieira[65], M. Vieites Diaz[49], H. Viemann[76], X. Vilasis-Cardona[85], E. Vilella Figueras[60], A. Villa[20], P. Vincent[13], F.C. Volle[11], D. Vom Bruch[10], A. Vorobyev[38], V. Vorobyev[43,v], N. Voropaev[38], K. Vos[80], R. Waldi[17], J. Walsh[29], C. Wang[17], J. Wang[5], J. Wang[4], J. Wang[3], J. Wang[73], M. Wang[3], R. Wang[54], Y. Wang[7], Z. Wang[50], Z. Wang[3], Z. Wang[6], J.A. Ward[56], N.K. Watson[53], S.G. Weber[13], D. Websdale[61], C. Weisser[64], B.D.C. Westhenry[54], D.J. White[62], M. Whitehead[54], A.R. Wiederhold[56], D. Wiedner[15], G. Wilkinson[63], M. Wilkinson[68], I. Williams[55], M. Williams[64], M.R.J. Williams[58], F.F. Wilson[57], W. Wislicki[36], M. Witek[35], L. Witola[17], G. Wormser[11], S.A. Wotton[55], H. Wu[68], K. Wyllie[48], Z. Xiang[6], D. Xiao[7], Y. Xie[7], A. Xu[5], J. Xu[6], L. Xu[3], M. Xu[7], Q. Xu[6], Z. Xu[5], Z. Xu[6], D. Yang[3], S. Yang[6], Y. Yang[6], Z. Yang[5], Z. Yang[66], Y. Yao[68], L.E. Yeomans[60], H. Yin[7], J. Yu[71], X. Yuan[68], O. Yushchenko[44], E. Zaffaroni[49], M. Zavertyaev[16,u], M. Zdybal[35], O. Zenaiev[48], M. Zeng[3], D. Zhang[7], L. Zhang[3], S. Zhang[71], S. Zhang[5], Y. Zhang[5], Y. Zhang[63], A. Zharkova[83], A. Zhelezov[17], Y. Zheng[6], T. Zhou[5], X. Zhou[6], Y. Zhou[6], V. Zhovkovska[11], X. Zhu[3], X. Zhu[7], Z. Zhu[6], V. Zhukov[14,40], J.B. Zonneveld[58], Q. Zou[4], S. Zucchelli[20,d], D. Zuliani[28], G. Zunica[62].

[1] *Centro Brasileiro de Pesquisas Físicas (CBPF), Rio de Janeiro, Brazil*
[2] *Universidade Federal do Rio de Janeiro (UFRJ), Rio de Janeiro, Brazil*
[3] *Center for High Energy Physics, Tsinghua University, Beijing, China*
[4] *Institute Of High Energy Physics (IHEP), Beijing, China*
[5] *School of Physics State Key Laboratory of Nuclear Physics and Technology, Peking University, Beijing, China*
[6] *University of Chinese Academy of Sciences, Beijing, China*
[7] *Institute of Particle Physics, Central China Normal University, Wuhan, Hubei, China*
[8] *Univ. Savoie Mont Blanc, CNRS, IN2P3-LAPP, Annecy, France*
[9] *Université Clermont Auvergne, CNRS/IN2P3, LPC, Clermont-Ferrand, France*
[10] *Aix Marseille Univ, CNRS/IN2P3, CPPM, Marseille, France*
[11] *Université Paris-Saclay, CNRS/IN2P3, IJCLab, Orsay, France*
[12] *Laboratoire Leprince-Ringuet, CNRS/IN2P3, Ecole Polytechnique, Institut Polytechnique de Paris, Palaiseau, France*
[13] *LPNHE, Sorbonne Université, Paris Diderot Sorbonne Paris Cité, CNRS/IN2P3, Paris, France*
[14] *I. Physikalisches Institut, RWTH Aachen University, Aachen, Germany*
[15] *Fakultät Physik, Technische Universität Dortmund, Dortmund, Germany*
[16] *Max-Planck-Institut für Kernphysik (MPIK), Heidelberg, Germany*
[17] *Physikalisches Institut, Ruprecht-Karls-Universität Heidelberg, Heidelberg, Germany*
[18] *School of Physics, University College Dublin, Dublin, Ireland*
[19] *INFN Sezione di Bari, Bari, Italy*
[20] *INFN Sezione di Bologna, Bologna, Italy*
[21] *INFN Sezione di Ferrara, Ferrara, Italy*
[22] *INFN Sezione di Firenze, Firenze, Italy*
[23] *INFN Laboratori Nazionali di Frascati, Frascati, Italy*
[24] *INFN Sezione di Genova, Genova, Italy*
[25] *INFN Sezione di Milano, Milano, Italy*
[26] *INFN Sezione di Milano-Bicocca, Milano, Italy*
[27] *INFN Sezione di Cagliari, Monserrato, Italy*
[28] *Universita degli Studi di Padova, Universita e INFN, Padova, Padova, Italy*
[29] *INFN Sezione di Pisa, Pisa, Italy*
[30] *INFN Sezione di Roma La Sapienza, Roma, Italy*

[31] *INFN Sezione di Roma Tor Vergata, Roma, Italy*
[32] *Nikhef National Institute for Subatomic Physics, Amsterdam, Netherlands*
[33] *Nikhef National Institute for Subatomic Physics and VU University Amsterdam, Amsterdam, Netherlands*
[34] *AGH - University of Science and Technology, Faculty of Physics and Applied Computer Science, Kraków, Poland*
[35] *Henryk Niewodniczanski Institute of Nuclear Physics Polish Academy of Sciences, Kraków, Poland*
[36] *National Center for Nuclear Research (NCBJ), Warsaw, Poland*
[37] *Horia Hulubei National Institute of Physics and Nuclear Engineering, Bucharest-Magurele, Romania*
[38] *Petersburg Nuclear Physics Institute NRC Kurchatov Institute (PNPI NRC KI), Gatchina, Russia*
[39] *Institute for Nuclear Research of the Russian Academy of Sciences (INR RAS), Moscow, Russia*
[40] *Institute of Nuclear Physics, Moscow State University (SINP MSU), Moscow, Russia*
[41] *Institute of Theoretical and Experimental Physics NRC Kurchatov Institute (ITEP NRC KI), Moscow, Russia*
[42] *Yandex School of Data Analysis, Moscow, Russia*
[43] *Budker Institute of Nuclear Physics (SB RAS), Novosibirsk, Russia*
[44] *Institute for High Energy Physics NRC Kurchatov Institute (IHEP NRC KI), Protvino, Russia, Protvino, Russia*
[45] *ICCUB, Universitat de Barcelona, Barcelona, Spain*
[46] *Instituto Galego de Física de Altas Enerxías (IGFAE), Universidade de Santiago de Compostela, Santiago de Compostela, Spain*
[47] *Instituto de Fisica Corpuscular, Centro Mixto Universidad de Valencia - CSIC, Valencia, Spain*
[48] *European Organization for Nuclear Research (CERN), Geneva, Switzerland*
[49] *Institute of Physics, Ecole Polytechnique Fédérale de Lausanne (EPFL), Lausanne, Switzerland*
[50] *Physik-Institut, Universität Zürich, Zürich, Switzerland*
[51] *NSC Kharkiv Institute of Physics and Technology (NSC KIPT), Kharkiv, Ukraine*
[52] *Institute for Nuclear Research of the National Academy of Sciences (KINR), Kyiv, Ukraine*
[53] *University of Birmingham, Birmingham, United Kingdom*
[54] *H.H. Wills Physics Laboratory, University of Bristol, Bristol, United Kingdom*
[55] *Cavendish Laboratory, University of Cambridge, Cambridge, United Kingdom*
[56] *Department of Physics, University of Warwick, Coventry, United Kingdom*
[57] *STFC Rutherford Appleton Laboratory, Didcot, United Kingdom*
[58] *School of Physics and Astronomy, University of Edinburgh, Edinburgh, United Kingdom*
[59] *School of Physics and Astronomy, University of Glasgow, Glasgow, United Kingdom*
[60] *Oliver Lodge Laboratory, University of Liverpool, Liverpool, United Kingdom*
[61] *Imperial College London, London, United Kingdom*
[62] *Department of Physics and Astronomy, University of Manchester, Manchester, United Kingdom*
[63] *Department of Physics, University of Oxford, Oxford, United Kingdom*
[64] *Massachusetts Institute of Technology, Cambridge, MA, United States*
[65] *University of Cincinnati, Cincinnati, OH, United States*
[66] *University of Maryland, College Park, MD, United States*
[67] *Los Alamos National Laboratory (LANL), Los Alamos, United States*
[68] *Syracuse University, Syracuse, NY, United States*
[69] *School of Physics and Astronomy, Monash University, Melbourne, Australia, associated to* [56]
[70] *Pontifícia Universidade Católica do Rio de Janeiro (PUC-Rio), Rio de Janeiro, Brazil, associated to* [2]
[71] *Physics and Micro Electronic College, Hunan University, Changsha City, China, associated to* [7]
[72] *Guangdong Provincial Key Laboratory of Nuclear Science, Guangdong-Hong Kong Joint Laboratory of Quantum Matter, Institute of Quantum Matter, South China Normal University, Guangzhou, China, associated to* [3]
[73] *School of Physics and Technology, Wuhan University, Wuhan, China, associated to* [3]
[74] *Departamento de Fisica , Universidad Nacional de Colombia, Bogota, Colombia, associated to* [13]
[75] *Universität Bonn - Helmholtz-Institut für Strahlen und Kernphysik, Bonn, Germany, associated to* [17]
[76] *Institut für Physik, Universität Rostock, Rostock, Germany, associated to* [17]
[77] *Eotvos Lorand University, Budapest, Hungary, associated to* [48]
[78] *INFN Sezione di Perugia, Perugia, Italy, associated to* [21]
[79] *Van Swinderen Institute, University of Groningen, Groningen, Netherlands, associated to* [32]

[80] *Universiteit Maastricht, Maastricht, Netherlands, associated to* [32]
[81] *National Research Centre Kurchatov Institute, Moscow, Russia, associated to* [41]
[82] *National Research University Higher School of Economics, Moscow, Russia, associated to* [42]
[83] *National University of Science and Technology "MISIS", Moscow, Russia, associated to* [41]
[84] *National Research Tomsk Polytechnic University, Tomsk, Russia, associated to* [41]
[85] *DS4DS, La Salle, Universitat Ramon Llull, Barcelona, Spain, associated to* [45]
[86] *Department of Physics and Astronomy, Uppsala University, Uppsala, Sweden, associated to* [59]
[87] *University of Michigan, Ann Arbor, United States, associated to* [68]

[a] *Universidade Federal do Triângulo Mineiro (UFTM), Uberaba-MG, Brazil*
[b] *Hangzhou Institute for Advanced Study, UCAS, Hangzhou, China*
[c] *Università di Bari, Bari, Italy*
[d] *Università di Bologna, Bologna, Italy*
[e] *Università di Cagliari, Cagliari, Italy*
[f] *Università di Ferrara, Ferrara, Italy*
[g] *Università di Firenze, Firenze, Italy*
[h] *Università di Genova, Genova, Italy*
[i] *Università degli Studi di Milano, Milano, Italy*
[j] *Università di Milano Bicocca, Milano, Italy*
[k] *Università di Modena e Reggio Emilia, Modena, Italy*
[l] *Università di Padova, Padova, Italy*
[m] *Scuola Normale Superiore, Pisa, Italy*
[n] *Università di Pisa, Pisa, Italy*
[o] *Università della Basilicata, Potenza, Italy*
[p] *Università di Roma Tor Vergata, Roma, Italy*
[q] *Università di Siena, Siena, Italy*
[r] *Università di Urbino, Urbino, Italy*
[s] *MSU - Iligan Institute of Technology (MSU-IIT), Iligan, Philippines*
[t] *AGH - University of Science and Technology, Faculty of Computer Science, Electronics and Telecommunications, Kraków, Poland*
[u] *P.N. Lebedev Physical Institute, Russian Academy of Science (LPI RAS), Moscow, Russia*
[v] *Novosibirsk State University, Novosibirsk, Russia*
[w] *Hanoi University of Science, Hanoi, Vietnam*